

## Tensile loading of Ti-25Nb-0.7O shape memory alloy monitored by infrared thermography and digital image correlation

by K. M. Golasinski\*, M. Maj\*\*, W. Tasaki\*\*\*, E. A. Pieczynska\*\* and H. Y. Kim\*\*\*

\* Multidisciplinary Research Center, Cardinal Stefan Wyszyński University in Warsaw, Dewajtis 5, Warsaw 01-815, Poland, [k.golasinski@uksw.edu.pl](mailto:k.golasinski@uksw.edu.pl)

\*\* Institute of Fundamental Technological Research, Polish Academy of Sciences, Pawińskiego 5 B, Warsaw 02-106, Poland, [mimaj@ippt.pan.pl](mailto:mimaj@ippt.pan.pl), [epiecz@ippt.pan.pl](mailto:epiecz@ippt.pan.pl)

\*\*\* Division of Materials Science, Faculty of Pure and Applied Sciences, University of Tsukuba, Tsukuba, Ibaraki 305-8573, Japan, [tasaki.wataru.fw@u.tsukuba.ac.jp](mailto:tasaki.wataru.fw@u.tsukuba.ac.jp), [heeykim@ims.tsukuba.ac.jp](mailto:heeykim@ims.tsukuba.ac.jp)

### Abstract

Thermomechanical behavior of a biomedical Ti-25Nb-0.7O (at. %) shape memory alloy was investigated by conducting a load-unload tensile test inspected by infrared thermography and digital image correlation. Global characteristics, namely stress and average temperature change vs. strain curves, served to identify specific deformation stages of the alloy. The stress vs. strain curve of the alloy indicated mechanical hysteresis during loading and a nonlinear superelastic unloading with a recoverable strain of around 0.021. The initial, linear, elastic deformation of Ti-25Nb-0.7O was accompanied by a temperature drop due to the thermoelastic effect. Subsequent superelastic loading was found to be exothermic. The final stage of loading involved plastic deformation characterized by a temperature growth at a very similar rate when compared to the superelastic loading. At the beginning of the unloading process, the temperature drop was fast and it ended with a slight increase of temperature. Local thermomechanical features, i.e. temperature and strain fields showed that the deformation of Ti-25Nb-0.7O was inhomogeneous since the beginning of the loading process. Furthermore, the technique of IRT was able to capture very instantaneous temperature changes of the Ti-25Nb-0.7O SMA during the hysteretic deformation. They can be directly associated with the dissipative behaviour of the underlying deformation mechanism of the superelastic Ti-25Nb-0.7O shape memory alloy.

**Keywords:** biomedical shape memory alloy, superelasticity, interstitial oxygen atoms, martensitic transformation, digital image correlation, infrared thermography.

### 1. Introduction

Nickel titanium (NiTi), also known as nitinol, is the most commonly used shape memory alloy (SMA) in commercial applications [1-3]. Nitinol can exhibit shape memory effect or superelasticity associated with the martensitic transformation from the cubic B2 parent phase to the monoclinic B19' martensite. It is macroscopically manifested by an inhomogeneous Lüders-type deformation during tensile loading [4]. The application of full-field measurement techniques for determination of the thermomechanical behavior of SMAs, was reviewed in [5]. The nucleation and propagation of phase transformation fronts in a NiTi SMA under deformation were studied using infrared thermography (IRT) [6-14] and digital image correlation (DIC) [15-17]. Nickel hypersensitivity has dictated the need to develop biomedical Ni-free Ti-Nb based SMAs, which can also exhibit shape memory effect or superelasticity associated with the martensitic transformation in this case from the cubic  $\beta$  parent phase to the orthorhombic  $\alpha'$  martensite [18-22]. The addition of oxygen to Ti-Nb SMAs can change the deformation mechanism of superelasticity in this class of SMAs into a continuous strain glass transition due to a specific nanosized lattice modulation (nanodomains) [23-25]. As a consequence, the addition of oxygen changes the stress-strain response of Ti-Nb-O SMAs.

Recently, macroscopic deformation of Ti-25Nb-xO (x=0; 0.3; 0.7, at.%) SMAs under tension was investigated using digital image correlation (DIC) in [26]. Strain fields of the SMAs determined at selected stages of tensile deformation up to around 3% showed that the Ti-25Nb SMA exhibits development of two macroscopic bands, whereas the Ti-25Nb-0.3O and Ti-25Nb-0.7 SMAs show a more discrete type of deformation in a form of very narrow bands. It is known, that high content of oxygen (over 1 at. %) causes a nonlinear superelastic behavior of Ti-Nb-O SMAs, as in the case of Gum Metal with composition Ti-23Nb-0.7Ta-2Zr-1.2O (at.%) [27-30]. Infrared thermography (IRT) and DIC were already successfully applied to investigate the thermomechanical behavior of Gum Metal under tensile monotonic [31, 32] and cyclic [33] loadings. However, only average temperature change values could contribute to a better understanding of thermomechanical behavior of Gum Metal under deformation. Specifically, it was found that the recoverable deformation of Gum Metal is composed of a linear elastic part accompanied by a temperature drop and a nonlinear part which causes a temperature growth. The superelastic unloading of Gum Metal was found to be thermomechanically reversible. No local effects were observed in strain or temperature fields determined at particular stages of the Gum Metal's deformation. Strain-rate sensitivity analysis based on the DIC study did not reveal local particularities in Gum Metal under tension either [34]. The goal of this study was to investigate the thermomechanical characteristics of Ti-25Nb-0.7O (at.%) SMA, which has a lower oxygen content than Gum Metal, under tensile loading using IRT and DIC.



## 2. Materials and methods

The Ti–25Nb–0.7O alloy was prepared by the Ar arc melting method using pre-melted sponges of Ti (99.9%) and pure Nb (99.9%). The oxygen concentration of the alloys was adjusted by the amount of powder TiO<sub>2</sub> (99.9%). The ingot was sealed in a vacuumed quartz tube and homogenized at 1273 K for 120 min, and then cold-rolled with a reduction in thickness of 95% (final thickness was 0.5 mm). Specimens for X-ray diffraction (XRD) measurements, scanning electron microscopy (SEM) and tensile testing were cut using an electro-discharge machine. The damaged surface was removed by mechanical polishing and chemical etching. The specimens were solution-treated at 1173 K for 30 min in an Ar atmosphere, followed by water quenching. The oxidized surface was removed by chemical etching. The surface of SEM samples was electropolished at 233 K using a solution of perchloric acid/butanol/methanol at 1:6:10 by volume. SEM observations were made using a JEOL JSM-IT300 device. XRD measurements were conducted at room temperature with Cu K $\alpha$  radiation using a Bruker D2 PHASER Benchtop device.

A technical drawing and a photograph of the tensile specimen are shown in Figs. 1(a) and 1(b), respectively. The gauge area of the specimen, with dimensions 4 mm x 6 mm, was covered with a speckle pattern for 2D DIC on one side and with sooth for IRT on the other side. An MTS 858 testing machine was used to perform a displacement-controlled load-unload tensile test at room temperature. The maximal displacement was 0.35 mm. The displacement rate was 0.06 mm·s<sup>-1</sup>. It corresponds to an average strain rate of 10<sup>-2</sup> s<sup>-1</sup>, when the specimen geometry is considered. During the deformation process, the specimen was observed by two synchronized cameras. The displacement and strain fields were obtained from the visible range image sequence captured by a visible range camera sCMOS PCO Edge 5.5 (image size 2560 px x 1046 px; pixel size 6.6  $\mu$ m; recording frequency 100 Hz).

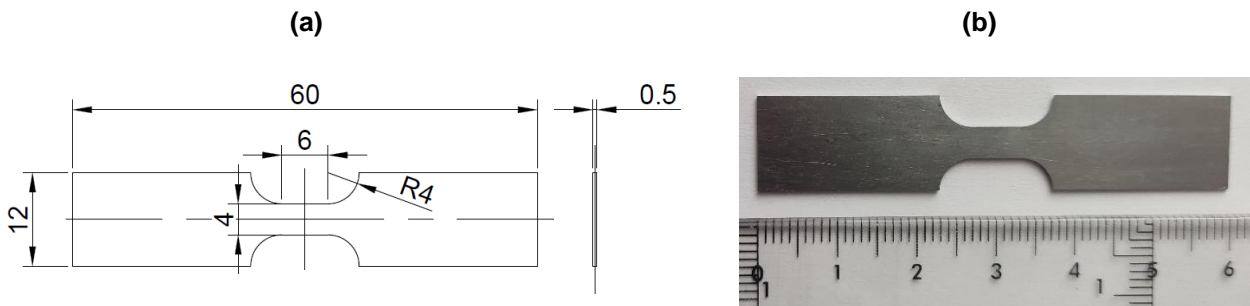


**Fig. 1.** (a) Technical drawing and (b) photograph of a Ti–25Nb–0.7O SMA tensile specimen.

The average strain values of the specimen under loading were determined on the basis of DIC results using a function of the virtual extensometer with an initial length of 6 mm. The data were calculated using a 2D DIC algorithm implemented in ThermoCorr software [35]. The temperature fields during the deformation of the Ti-25Nb-0.7O SMA were obtained based on the infrared radiation emitted from the specimen's surface and registered by a ThermoCam Phoenix IR camera (image size 320 px x 256 px; pixel size 40  $\mu$ m; recording frequency 100 Hz).

The mean temperature was determined with high thermal sensitivity up to 0.02 °C based on the obtained temperature distribution from the gauge area of the specimen. The temperature change  $\Delta T$  was calculated using the equation Eq.1.

$$\Delta T = T(t) - T(t_0), \quad (\text{Eq. 1})$$

where

$T(t)$  is the mean value of the temperature calculated for the gauge area of the specimen at each instant of straining

$T(t_0)$  is the mean temperature of the same area before the deformation.

This experimental methodology was already successfully applied for thermomechanical studies of stainless steel [36] and Gum Metal [31-33] under deformation.

### 3. Results and discussion

Stress, strain and temperature change vs. time curves of Ti–25Nb–0.7O SMA under load-unload tension are shown in Fig. 2. The deformation process was not fully reversible as indicated by the strain remained after unloading greater than 0.01.

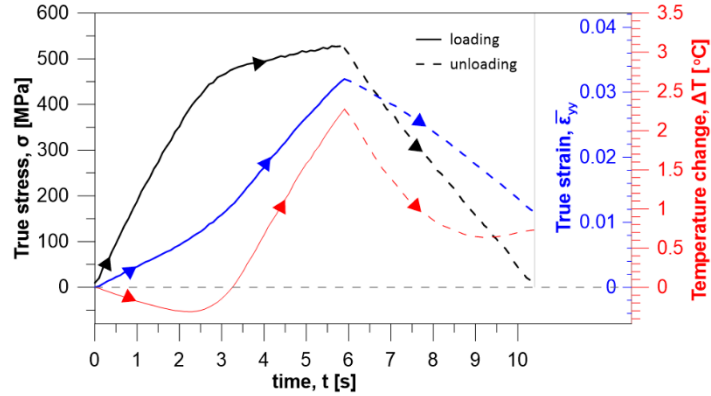


**Fig. 2.** Stress, strain and temperature change vs. time curves of Ti–25Nb–0.7O SMA under load-unload tension.

XRD profiles of as-fabricated and as-deformed Ti–25Nb–0.7O SMA showed peaks corresponding only to beta phase, as seen in Fig. 3. SEM micrographs of as-fabricated and as-deformed Ti–25Nb–0.7O SMA are presented in Fig. 4(a) and 4(b), respectively. The microstructure of the as-fabricated alloy revealed beta phase grains. However, the microstructure of the as-deformed Ti–25Nb–0.7O SMA showed lamella structures, which are most probably twins produced during the plastic deformation. This observation is in line with studies on plastic deformation mechanisms in metastable beta titanium alloys [37-39].

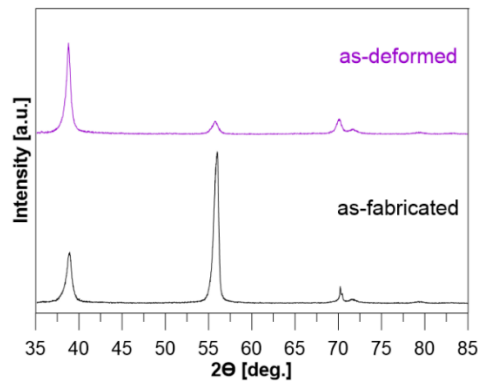


**Fig. 3.** XRD diffractograms of as-fabricated and as-deformed Ti–25Nb–0.7O SMA.

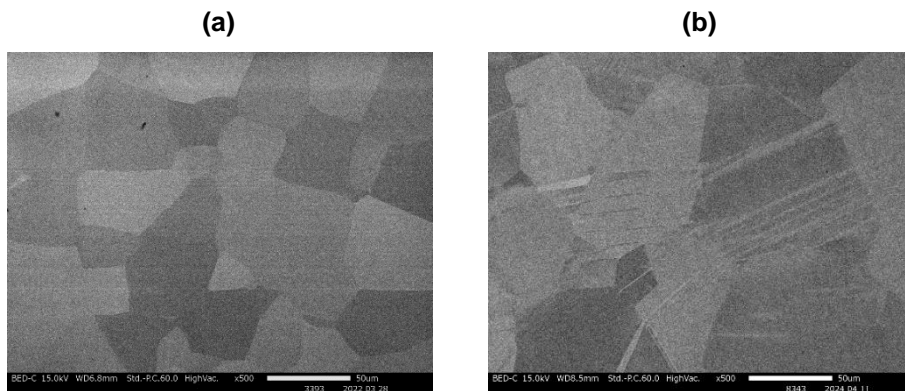


**Fig. 4.** SEM images of (a) as-fabricated and (b) as-deformed Ti–25Nb–0.7O SMA.

Stress vs. strain curve of Ti–25Nb–0.7O SMA under load-unload tension is shown in Fig. 3(a). It indicates a clear mechanical hysteresis. The recovery strain  $\bar{\epsilon}_r = 0.021$  can be determined based on the unloading stress vs. strain curve. Stress and temperature change vs. strain curves of Ti–25Nb–0.7O SMA under tensile loading are shown in Fig. 3(b).

According to the formula proposed by W. Thomson [40], during the adiabatic, elastic deformation under assumption of linear and isotropic elastic behavior of solid material, the temperature change can be described by Eq. 2.

$$\Delta T = -\frac{\alpha T \text{tr} \sigma}{c_p \rho}, \quad (\text{Eq. 2}),$$

where

$\alpha$  is the coefficient of linear thermal expansion,  
 $T$  is the absolute temperature of the specimen,  
 $\text{tr} \sigma$  is the trace of stress tensor  $\sigma$ ,  
 $c_p$  is the specific heat at constant pressure and  
 $\rho$  is the density of the material.

Thus, in the case of conventional alloys subjected to tension, the minimum temperature change can be an indicator of the yield stress at which the material begins to deform plastically [41, 42]. It was experimentally proven for instance for stainless steel in [43-45], IMI-834 titanium alloy [46], titanium grade 2 and aluminum [47]. In the case of SMAs, the minimum temperature change corresponds to the yield stress at which the material begins to deform via phase transformation [8-14]. In Fig. 3(b), three methods for yield stress determination were compared. A proportionality limit  $YS_{ap} = 293 \text{ MPa}$  and an 0.2% offset yield stress  $YS_{0.2\%} = 470 \text{ MPa}$  were identified based on the stress vs. strain curve only. The maximum temperature drop  $\Delta T_{min} = -0.31 \text{ }^\circ\text{C}$  of the Ti–25Nb–0.7O SMA specimen under tension can indicate another yield stress value  $YS_{Tmin} = 399 \text{ MPa}$ .

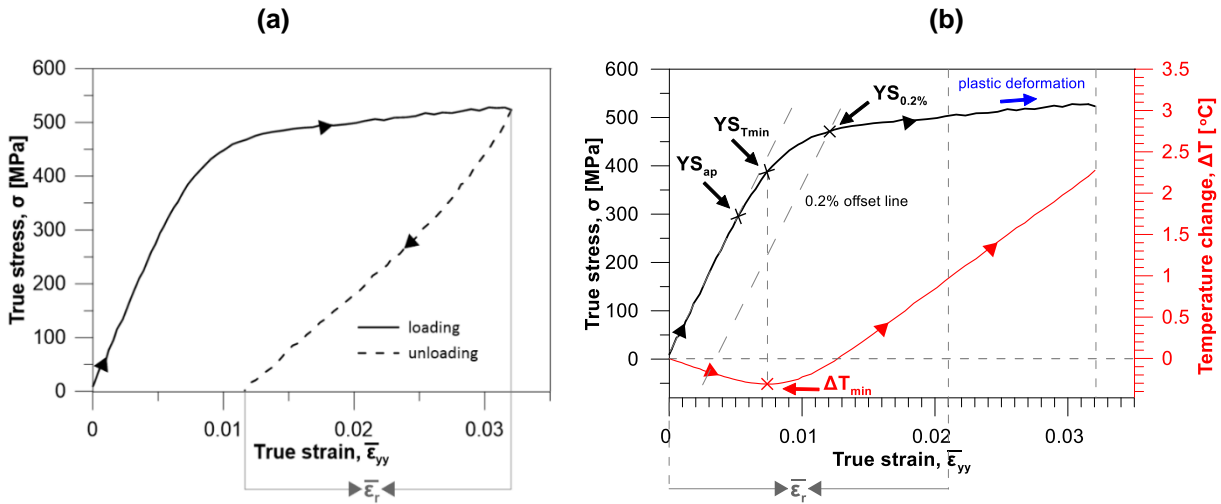


**Fig. 5.** (a) Stress vs. strain curve of Ti–25Nb–0.7O SMA under load-unload tension and (b) yield stress determination based on stress and temperature change vs. strain curves of Ti–25Nb–0.7O SMA during tensile loading.

Further deformation of Ti–25Nb–0.7O SMA, recoverable until  $\bar{\epsilon}_r = 0.021$ , is accompanied by a temperature growth. Then, the plastic deformation with a continuous temperature growth starts. Critical parameters determined based on the stress and temperature change vs. strain curves of Ti–25Nb–0.7O SMA during tensile loading are listed in Table 1.

**Table 1.** Yield stress values  $YS_{ap}$ ,  $YS_{0.2\%}$  and  $YS_{Tmin}$  determined based on stress and temperature change vs. strain curves of Ti–25Nb–0.7O SMA during tensile loading

Yield stress	$YS_{ap}$	$YS_{0.2\%}$	$YS_{Tmin}$
Value	293 MPa	470 MPa	399 MPa

Stress and temperature change vs. strain curves of the Ti–25Nb–0.7O SMA under load-unload tension with strain  $\epsilon_{yy}$  (A)-(E) and temperature change  $\Delta T$  (A\*)-(E\*) fields determined at selected stages of the loading process are presented in Fig. 6.

The stages correspond to the following values of  $\bar{\varepsilon}_{yy}$  during loading:

- (1)  $\bar{\varepsilon}_{yy} = 0.005$
- (2)  $\bar{\varepsilon}_{yy} = 0.008$
- (3)  $\bar{\varepsilon}_{yy} = 0.010$
- (4)  $\bar{\varepsilon}_{yy} = 0.020$
- (5)  $\bar{\varepsilon}_{yy} = \bar{\varepsilon}_{max}$ .

The  $\varepsilon_{yy}$  fields show that the Ti–25Nb–0.7O SMA deforms in an inhomogeneous manner since the beginning of the loading process (A)-(B) in a form of very narrow bands. The  $\Delta T$  fields reveal that the initial part of deformation is accompanied by a temperature drop 0-(A\*)-(B\*). Between stages (A)-(C), there is an apparent yield point, which can be determined in (B) based on the maximum temperature drop (B\*), as discussed previously. Temperature starts to increase between (B\*)-(C\*). During an advanced stage of loading (C)-(D)-(E) three zones with significant values of  $\varepsilon_{yy}$  with adjacent  $\Delta T$  growth (C\*)-(D\*)-(E\*) develop. From Fig. 2(a), we know that the recoverable strain of Ti–25Nb–0.7O SMA is  $\bar{\varepsilon}_r = 0.021$ . Thus, it can be estimated that the Ti–25Nb–0.7O SMA deforms in a recoverable manner between 0-(D).

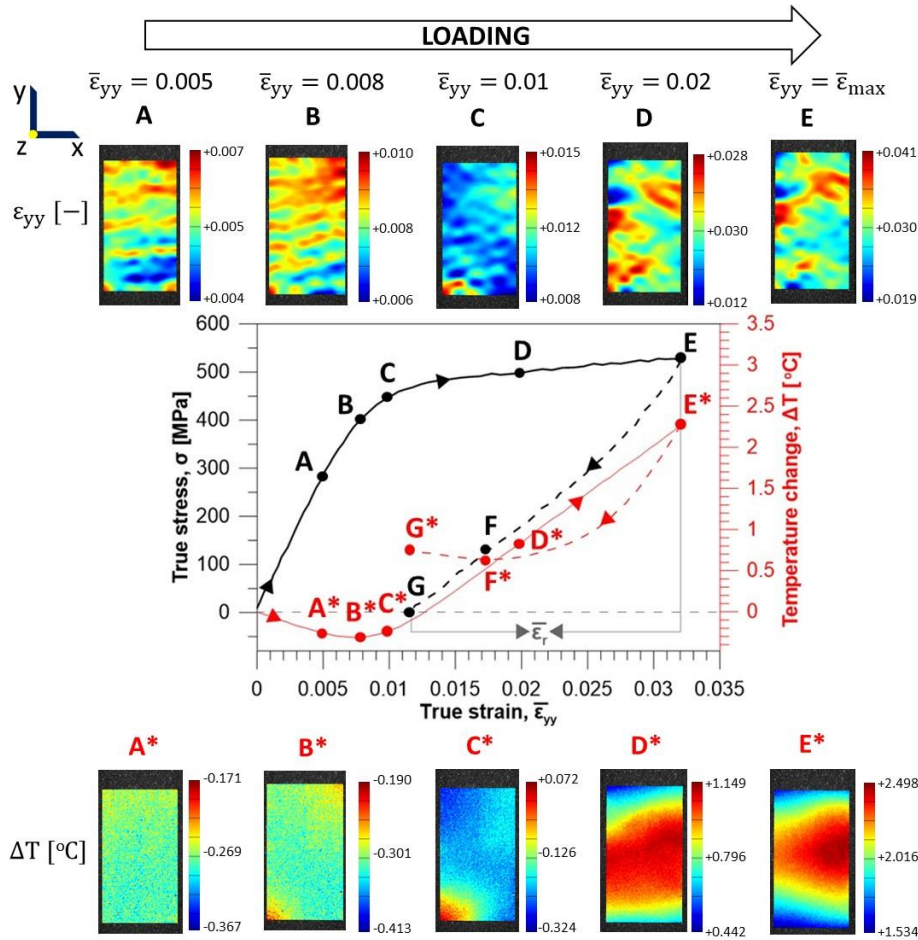


**Fig. 6.** Stress and temperature change vs. strain curves of the Ti–25Nb–0.7O SMA under tension with  $\varepsilon_{yy}$  and  $\Delta T$  fields determined at selected stages of the loading process.

At the beginning of the loading process 0-(B), a drop of temperature 0-(B\*) occurs due to the thermoelastic effect. However, subsequently a temperature increase (B\*)-(D\*) can be observed. During unloading (E)-(F), the temperature first rapidly decreases (E\*)-(F\*) and then slightly increases (F\*)-(G\*). It proves that the superelasticity of oxygen-added Ti-Nb SMAs, associated with a specific lattice modulation, is exothermic during loading and endothermic during unloading, as in the case of Gum Metal [31-33]. It is also worth to note that the increase of temperature related to the plastic deformation (D)-(E) involving mechanical twinning (see Fig. 4(b)) proceeds at a very similar rate when compared with the temperature growth (B\*)-(D\*) linked to the superelastic deformation (B)-(D) caused by the strain glass transition. In the case of Gum Metal, the temperature growth associated with the plastic deformation was faster than that related to superelasticity [31-33]. This difference is caused by different mechanisms of plastic deformation of the Ti–25Nb–0.7O SMA and Gum Metal. Dominant deformation stages of the Ti–25Nb–0.7O SMA identified during load-unload tension with the accompanying temperature change are listed in Table 2.

**Table 2.** Dominant deformation stages of the Ti–25Nb–0.7O SMA identified during load-unload tension with the accompanying temperature change.

Dominant deformation stage		Temperature change	
(0)-(B)	ELASTIC LOADING	(0)-(B*)	Slight drop
(B)-(D)	SUPERELASTIC LOADING	(B*)-(D*)	Moderate growth
(D)-(E)	PLASTIC LOADING	(D*)-(E*)	Moderate growth
(E)-(F)	SUPERELASTIC UNLOADING	(E*)-(F*)	Fast drop
(F)-(G)	ELASTIC UNLOADING	(F*)-(G*)	Slight growth

In general the  $\Delta T$  fields show that local values of temperature determined at selected stages of the Ti–25Nb–0.7O SMA loading directly correspond to the local strain  $\varepsilon_{yy}$ . However the  $\Delta T$  fields were more blurred, whereas the  $\varepsilon_{yy}$  fields gave quite a detailed description of the inhomogeneity of the tensile process. Particularly, at the beginning of the loading process, the  $\varepsilon_{yy}$  fields showed deformation in a form of very narrow bands. No additional particular effects can be distinguished either in the  $\Delta T$  or  $\varepsilon_{yy}$  fields presented in Fig. 6. A comparison of  $\varepsilon_{yy}$  and  $\Delta T$  fields of the Ti–25Nb–0.7O SMA captured at slightly different stages of the loading process corresponding to  $\bar{\varepsilon}_{yy} = 0.011$ ,  $\bar{\varepsilon}_{yy} = 0.016$  and  $\bar{\varepsilon}_{yy} = 0.021$  is shown in Fig. 7.

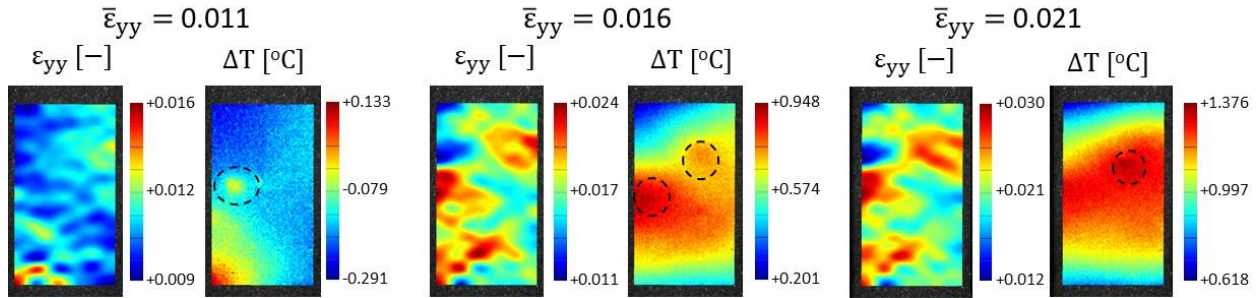


**Fig. 7.**  $\varepsilon_{yy}$  and  $\Delta T$  fields of the Ti–25Nb–0.7O SMA under tension determined at  $\bar{\varepsilon}_{yy} = 0.011$ ,  $\bar{\varepsilon}_{yy} = 0.016$  and  $\bar{\varepsilon}_{yy} = 0.021$ .

It reveals an abrupt temperature growth in circled zones. These discrete changes of temperature occurring during the superelastic deformation of the Ti–25Nb–0.7O SMA can be associated with the hysteretic behaviour caused by a continuous strain glass transition due to the lattice modulation caused by the oxygen interstitials [23-25]. They are not apparent in the corresponding  $\varepsilon_{yy}$  fields presented in Fig. 7.

#### 4. Conclusions

The analysis of the thermomechanical behavior of the Ti-25Nb-0.7O SMA under load-unload tension was performed using synchronized techniques of IRT and DIC. Based on the results obtained in this work, the following conclusions can be drawn.

- 1) The average temperature change can successfully serve to identify specific deformation stages of the Ti-25Nb-0.7O SMA, which include a linear elastic deformation accompanied by a temperature drop followed by superelastic and plastic deformation regimes of exothermic nature,
- 2) The deformation of the Ti-25Nb-0.7O SMA under tension was found to be inhomogeneous since the beginning of the loading process as demonstrated in  $\varepsilon_{yy}$  and  $\Delta T$  fields. The  $\varepsilon_{yy}$  fields gave quite a detailed description of the inhomogeneity of the tensile process, whereas the  $\Delta T$  fields were more blurred.
- 3) The technique of IRT was able to capture very instantaneous temperature changes of the Ti-25Nb-0.7O SMA under tensile loading. These local effects were not evident in the  $\varepsilon_{yy}$  fields determined by DIC. It suggests that they are directly associated with the dissipative behaviour of the underlying deformation mechanism of the super-elastic Ti-25Nb-0.7O SMA.

#### Acknowledgements

Karol M. Golasiński acknowledges the support of the Japan Society for the Promotion of Science (JSPS) Postdoctoral Fellowship (ID No. P20812). This research was funded in part by the National Science Centre, Poland through the Grant 2023/48/C/ST8/00038. The authors express their gratitude to Leszek Urbański (IPPT PAN) for conducting tension test.

## Disclosure Statement

The authors report there are no competing interests to declare.

## References

- [1] Duerig T, Pelton A, Stöckel D. An overview of nitinol medical applications, *Mater Sci Eng A*. 1999;273–275:149-160.
- [2] Morgan NB. Medical shape memory alloy applications—the market and its products, *Mater Sci Eng A*. 2004;378: 16-23.
- [3] Jani J, Leary M, Subic A, Gibson MA. A review of shape memory alloy research, applications and opportunities, *Mater Des*. 2014;56:1078-1113.
- [4] Miyazaki S, Imai T, Otsuka K, Suzuki Y. Lüders-like deformation observed in the transformation pseudoelasticity of a Ti-Ni alloy, *Scripta Metall*. 1981;15:853-856.
- [5] Delpueyo D, Jury A, Balandraud X, Grédiac M. Applying Full-Field Measurement Techniques for the Thermomechanical Characterization of Shape Memory Alloys: A Review and Classification. *Shap Mem Superelasticity*. 2021;7:462–490.
- [6] Shaw JA, Kyriakides S. Thermomechanical aspects of NiTi, *J Mech Phys Solids*. 1995;43:1243-1281.
- [7] Shaw JA, Kyriakides S. On the nucleation and propagation of phase transformation fronts in a NiTi alloy, *Acta Mater*. 1997;45:683-700.
- [8] Pieczyska EA, Gadaj SP, Nowacki WK, Tobushi H. Thermomechanical investigations of martensitic and reverse transformations in TiNi shape memory alloy. *Bull. Pol. Acad. Sci. Tech. Sci*. 2004;52(3):165–171.
- [9] Gadaj SP, Nowacki WK, Pieczyska EA, Tobushi H. Temperature measurement as a new technique applied to the phase transformation study in a TiNi shape memory alloy subjected to tension. *Arch Metall Mater*. 2005;50(3):661–674.
- [10] Pieczyska EA, Gadaj SP, Nowacki WK, Tobushi H. Phase-Transformation Fronts Evolution for Stress- and Strain-Controlled Tension Tests in TiNi Shape Memory Alloy. *Exp Mech*. 2006;46(4):531–542.
- [11] Pieczyska EA. Activity of stress-induced martensite transformation in TiNi shape memory alloy studied by infrared technique. *J Mod Opt*. 2010;57(18):1700–1707.
- [12] Pieczyska EA, Tobushi H, Kulasiński K. Development of transformation bands in TiNi SMA for various stress and strain rates studied by a fast and sensitive infrared camera. *Smart Mater Struct*. 2013;22(3):035007-1-8.
- [13] Pieczyska EA, Gadaj SP, Nowacki WK, Tobushi H. Investigation of nucleation and propagation of phase transitions in TiNi SMA, *Quant InfraRed Thermogr J*. 2004;1-1:117-127.
- [14] Louche H, Chrysochoos A. Thermal and dissipative effects accompanying Lüders band propagation. *Mater Sci Eng A*. 2001;307(1-2):15–22.
- [15] Daly S, Ravichandran G, Bhattacharya K, Stress-induced martensitic phase transformation in thin sheets of Nitinol, *Acta Mater*. 2007;55:3593-3600.
- [16] Bewerse C, Gall KR, McFarland GJ, Zhu P, Brinson LC. Local and global strains and strain ratios in shape memory alloys using digital image correlation, *Mater Sci Eng A*. 2013;568:134-142.
- [17] Elibol C, Wagner M.F.-X., Investigation of the stress-induced martensitic transformation in pseudoelastic NiTi under uniaxial tension, compression and compression–shear, *Mater Sci Eng A*. Volume 621, Pages 76-81, 2015
- [18] Kim HY, Ikehara Y, Kim JI, Hosoda H, Miyazaki S, Martensitic transformation, shape memory effect and superelasticity of Ti–Nb binary alloys, *Acta Mater*. 2006;54:2419-2429.
- [19] Niinomi M, Nakai M, Hieda J. Development of new metallic alloys for biomedical applications, *Acta Biomater*. 2012;8:3888-3903.
- [20] Miyazaki S, Kim HY, Hosoda H. Development and characterization of Ni-free Ti-base shape memory and super-elastic alloys, *Mater Sci Eng A*. 2006;438–440:18-24.
- [21] Kim HY, Miyazaki S. Several Issues in the Development of Ti–Nb-Based Shape Memory Alloys, *Shap Mem Superelasticity*. 2016;2:380–390.
- [22] Yamauchi K, Ohkata I, Tsuchiya K, Miyazaki S (Editors), *Shape Memory and Superelastic Alloys Applications and Technologies*, Woodhead Publishing, 2011.
- [23] Tahara M, Kim HY, Inamura T, Hosoda H, Miyazaki S, Lattice modulation and superelasticity in oxygen-added  $\beta$ -Ti alloys, *Acta Mater*. 2011;59:6208-6218.
- [24] Wei LS, Kim HY, Miyazaki S. Effects of oxygen concentration and phase stability on nano-domain structure and thermal expansion behavior of Ti–Nb–Zr–Ta–O alloys, *Acta Mater*. 2015;100:313–322.
- [25] Wei LS, Kim HY, Koyano T, Miyazaki S. Effects of oxygen concentration and temperature on deformation behavior of Ti–Nb–Zr–Ta–O alloys. *Scr Mater*. 2016;123: 55–58.
- [26] Golasiński KM, Maj M, Tasaki W, Pieczyska EA, Kim HY. Full-field deformation study of Ti-25Nb, Ti-25Nb-0.3O and Ti-25Nb-0.7O shape memory alloys during tension using digital image correlation. *Metallurgical and Materials Transactions A*. 2024:1-10.
- [27] Saito T, Furuta T, Hwang JH, Kuramoto S, Nishino K, Suzuki N, Chen R, Yamada A, Ito K, Seno Y, Nonaka T, Ikehata H, Nagasako N, Iwamoto C, Ikuhara Y, Sakuma T. Multifunctional Alloys obtained via a dislocation free plastic deformation mechanism. *Science*. 2003;300(5618):464–467.
- [28] Kuramoto S, Furuta T, Hwang J, Nishino K, Saito T. Elastic properties of Gum Metal. *Mater Sci Eng A*. 2006;442(1-2):454–457.

- [29] Kuramoto S, Furuta T, Hwang JH, Nishino K, Saito T. Plastic deformation in a multifunctional Ti-Nb-Ta-Zr-O alloy. *Metall Mater Trans A*. 2006;37:657–662.
- [30] Furuta T, Kuramoto S, Morris JW, Nagasako N, Withey E, Chrzan DC. The mechanism of strength and deformation in Gum Metal. *Scr Mater*. 2013;68(10):767–772.
- [31] Golasiński KM, Pieczyska EA, Staszczak M, Maj M, Furuta T, Kuramoto S. Infrared thermography applied for experimental investigation of thermomechanical couplings in Gum Metal. *Quant Infrared Thermogr J*. 2017;14(2):226–233.
- [32] Pieczyska EA, Maj M, Golasiński KM, Staszczak M, Furuta T, Kuramoto S. Thermomechanical studies of yielding and strain localization phenomena of Gum Metal under tension. *Materials*. 2018;11(4):567.
- [33] Golasiński K, Maj M, Urbański L, Staszczak M, Gradys AD, Pieczyska EA. Experimental study of thermomechanical behaviour of Gum Metal during cyclic tensile loadings: the quantitative contribution of IRT and DIC. *Quant Infrared Thermogr J*. 2023.pp.1-18.
- [34] Golasiński K, Pieczyska E, Maj M, Staszczak M, Świec P, Furuta T, Kuramoto S. Investigation of strain rate sensitivity of Gum Metal under tension using digital image correlation. *Arch Civ Mech Eng*. 2020;20:53.
- [35] Nowak M, Maj M. Determination of coupled mechanical and thermal fields using 2D digital image correlation and infrared thermography: Numerical procedures and results. *Arch Civ Mech Eng*. 2018;18:630-644.
- [36] Musiał S, Maj M, Urbański L, Nowak M. Field analysis of energy conversion during plastic deformation of 310S stainless steel. *Int J Solids Struct*. 2022;238:111411.
- [37] Hanada S, Izumi O. Transmission electron microscopic observations of mechanical twinning in metastable beta titanium alloys. *Metall Trans A* 17, 1409–1420 (1986).
- [38] Tobe H, Kim HY, Inamura T, Hosoda H, Miyazaki S. Origin of {332} twinning in metastable  $\beta$ -Ti alloys, *Acta Mater*. 2014;64:345-355.
- [39] Yang Y, Zhang B, Meng Z, Qu L, Wang H, Cao S, Hu J, Chen H, Wu S, Ping D, Li G, Zhang LC, Yang R, Huang A. {332}<113> Twinning transfer behavior and its effect on the twin shape in a beta-type Ti-23.1Nb-2.0Zr-1.0O alloy. *J Mater Sci Technol*. 2021;91:58-66.
- [40] Thomson W. (Lord Kelvin). On the thermoelastic and thermomagnetic properties of matter. *Trans. R. Soc. Edinburgh*. 1853;20(161):57–77.
- [41] Chrysochoos A, Huon V, Jourdan F, Muracciole J-M, Peyroux R, Wattrisse B. Use of full-field digital image correlation and infrared thermography measurements for the thermomechanical analysis of material behaviour. *Strain*. 2010;46:117-130.
- [42] Beghi MG, Bottani CE, Caglioti G. Irreversible thermodynamics of metals under stress. *Res Mech*. 1986;19:365–379.
- [43] Pieczyska EA, Gadaj SP, Nowacki W. Investigation of thermomechanical coupling in an austenitic steel subjected to subsequent tensile deformation. *Proc 11th Int Conf Exp Mech*. 1998;681–685.
- [44] Pieczyska EA. Thermoelastic effect in austenitic steel referred to its hardening. *J Theor Appl Mech*. 1999;37(2)349–368.
- [45] Pieczyska EA, Gadaj SP, Nowacki WK. Thermoelastic and thermoplastic effects investigated in steel, polyamide and shape memory alloys. *Proc SPIE, Thermosense XXIV*. 2002;4710:479–497.
- [46] Kumar J, Baby S, Kumar V. Thermographic studies on IMI-834 titanium alloy during tensile loading. *Mater Sci Eng A*. 2008;496(1-2):303–307.
- [47] Oliferuk W, Maj M, Litwinko R, Urbański L. Thermomechanical coupling in the elastic regime and elasto-plastic transition during tension of austenitic steel, titanium and aluminium alloy at strain rates from  $10^{-4}$  to  $10^{-1} \text{ s}^{-1}$ . *Eur J Mech A Solids*. 2012;35:111–118.